Available online at www.sciencedirect.com
SCIENCE DIRECT
Polymer 46 (2005) 2257–2265
polymer
www.elsevier.com/locate/polymer

# Three-dimensional large-strain tensile deformation of neat and calcium carbonate-filled high-density polyethylene

E.M. Parsons[a], M.C. Boyce[a,*], D.M. Parks[a], M. Weinberg[b]

[a]*Department of Mechanical Engineering, Massachusetts Institute of Technology, Room 1-307, Cambridge MA 02139, USA*
[b]*E.I. du Pont de Nemours and Co., Central Research and Development, Experiment Station, Wellington DE 19898, USA*

Received 26 July 2004; received in revised form 10 December 2004; accepted 20 January 2005

**Abstract**

The large-strain tensile deformation of high-density polyethylene and high-density polyethylene filled with two volume fractions ($f$) of calcium carbonate particles is studied via an optical method. Digital image correlation is used to determine the local displacement gradients and full-field displacements during uniaxial tension tests on specimens of rectangular cross-section. A novel technique measures simultaneously, with a single camera, the deformation in all three dimensions. Full-field strain contours, macroscopic true stress-true strain behavior, and local volumetric strains are reduced from the raw test data. The true stress-true strain data shows an increase in modulus, but a decrease in yield stress and subsequent strain hardening, with increasing $f$. These results are strong evidence of particle debonding and are corroborated by an increase in volumetric strain with increasing $f$.


*Keywords:* Rigid-filled polymer; Tensile testing; Volumetric strain

## 1. Introduction

During a uniaxial tension test, most engineering polymers begin to deform inhomogeneously ('neck') at relatively small strains. Once necking begins, traditional extensometry methods provide little useful information. A contacting extensometer measures only the average strain over a gage length by tracking the relative position of two points on the specimen. Until the neck stabilizes and propagates the length of the specimen, however, the strain varies with axial position on the specimen. For this reason, polymer tensile stress-strain data is often limited to small strains, and little is known about the post-yield tensile behavior of polymers. The macroscopic data typically measured, nominal stress versus machine crosshead displacement, does not capture the local characteristics of the deformation. In order to determine the true stress-true strain behavior after the onset of necking, one must measure the local displacement field.

In both their neat and filled forms, many polymers increase in volume during tensile extension. Volumetric strain is important to measure because it is a key macroscopic indicator of microscopic deformation processes. In homopolymers, small-scale internal fracture processes such as crazing (glassy polymers) or crystal fragmentation (semi-crystalline polymers) are manifested by volumetric strain. In filled polymers, the debonding of rigid particulate fillers or the cavitation of elastomeric fillers allows void growth, an additional source of volumetric strain. Debonding and cavitation are important events to quantify as they are considered a critical ingredient to toughening, acting to relieve stress triaxiality and enable dissipative plastic flow.

The presence of significant volumetric strain complicates the calculation of the true stress (load per current cross-sectional area) in the specimen during the tensile test. Traditional tensile testing techniques measure the axial strain and approximate the current cross-sectional area of the specimen by assuming the volume of each material point of the specimen to be constant. If the volumetric strain is not negligible, however, this assumption causes the true stress

* Corresponding author. Tel.: +1 617 253 2342; fax: +1 617 258 8742.
*E-mail address:* mcboyce@mit.edu (M.C. Boyce).

0032-3861/$ - see front matter © 2005 Elsevier Ltd. All rights reserved.
doi:10.1016/j.polymer.2005.01.045

to be overestimated. The determination of the true stress at a given axial location on the specimen, therefore, requires knowledge of the actual cross-sectional area at that location. Displacements and strains must be measured not only in the axial direction but also in one (if transversely isotropic deformations may be assumed) or both lateral directions.

Any method that endeavors to measure local strains in inhomogeneously deforming polymers at moderate to large strains must either use an infinitesimally small gage length or, more practically, evaluate pointwise gradients in the displacement field. One technique that has been shown to be very effective in measuring displacements and displacement gradients is digital image correlation (DIC). DIC is the process of matching subsets of pixel gray-value patterns from one image to another. When DIC is applied to a mechanical test, an image of the undeformed specimen is correlated to an image of the deformed specimen, and the in-plane displacements and displacement gradients are calculated for one or more pixel subsets. From the displacement field or the displacement gradients, the strain measures are determined. A previous communication by Parsons et al. [1] describes in detail the application of DIC to the measurement of strains during the large-strain deformation of polymers. (A simplified version of this technique was utilized in the current authors' laboratory by Thio et al. [2] to quantify debonding in polypropylene toughened with rigid particles).

As summarized in Parsons et al., a number of investigators have used non-contacting, imaging methods to measure the large-strain deformation of polymers during uniaxial tension [3–9]. Some [9] have even used a form of DIC. The previous communication demonstrated how to reduce the desired stress and strain quantities from raw two-dimensional DIC data. The method described herein is unique in that it is capable of measuring full-field displacements and strains in all three dimensions with a single camera. As a result, a wealth of information is available, and there is no need to resort to assumptions of constant volume or transverse isotropy. True stress–true strain behavior at moderate to large strains can be thus determined for even the most inhomogeneously deforming polymers. Full-field strain contours and volumetric strain data provide further valuable insight into the mechanisms of deformation.

## 2. Procedure

### 2.1. Sample preparation

The material used in this study was high-density polyethylene (HDPE), trade name Dowlex IP-10, supplied by Dow Chemical Co. The neat polymer and blends containing, by volume, 10% and 20% calcium carbonate particles were tested. The particles, trade name Hi-Pflex 100, manufactured by Specialty Minerals Inc., had a mean diameter of 3.50 μm and were surface-treated by the supplier with calcium stearate. The neat polymer and blends were injection-molded into 12.7 mm × 3.2 mm × 144 mm bars. The mixing and molding process was conducted similarly to the method reported by Bartczak et al. [10,11]. Tensile specimens (shown in Fig. 1) with gage section dimensions 19.05 mm × 7.62 mm × 3.20 mm were machined from the molded bars.

### 2.2. Testing procedure

All tensile tests were conducted on an Instron model 5582 screw machine at a constant nominal strain rate of $0.005\ s^{-1}$. A random speckle pattern was applied to each specimen with a Badger airbrush filled with India ink. The pattern density was maximized under the constraint that individual speckles should generally not overlap. The minimum characteristic speckle size was three pixels (approximately 0.1 mm). High resolution (1280 pixels × 1024 pixels), 12-bit images were recorded at a frequency of 4 Hz with a Qimaging Retiga 1300 CCD camera equipped with a 200 mm f/4.0 Canon lens. The camera was placed at a distance of 1.0 m from the specimen. It was not assumed that the specimens would deform isotropically in the two lateral directions. Therefore, as shown in Fig. 1, the tests were viewed from two orientations; the 'front' view captured the deformation of the thick lateral dimension ($x$) and the 'side' view captured the deformation of the thin lateral dimension ($z$). Following the work of Roux et al. [12], the two views were recorded simultaneously in the same image by utilizing a right-angle prism. Fig. 2 is a schematic of the experimental set-up. The camera captured the front view of the specimen directly. The right-angle prism reflected light from the side view 90°, allowing both views to appear in the same image. As shown in Fig. 3, a fixture positioned the prism 12 mm from the side of the specimen. The load from the Instron load cell at the time of each image acquisition was recorded with a National

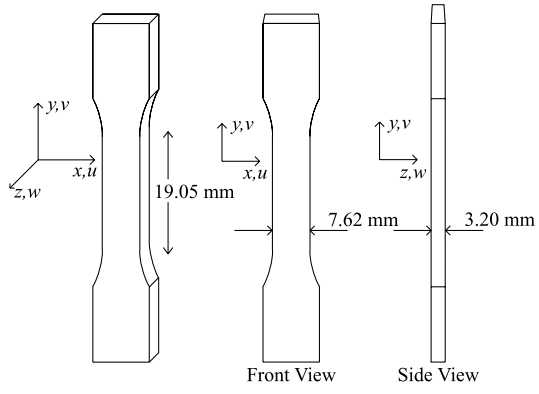


Fig. 1. Specimen geometry and definition of views and coordinate directions. $u$, $v$ and $w$ denote the displacements in the $x$, $y$ and $z$ directions, respectively.

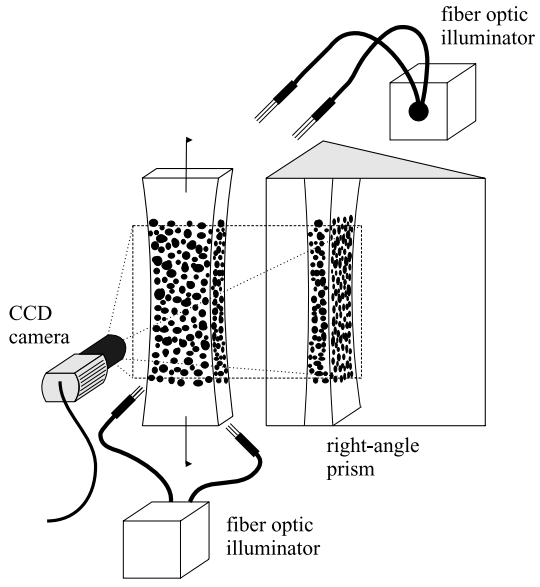


Fig. 2. Schematic of experimental set-up (not to scale).

Instruments DAQ board. Fig. 4 shows a reference image (a) and three deformed images (b–d).

### 2.3. Strain measurement

Displacements and strains were evaluated at individual points on the surfaces of the specimens. As shown in Fig. 4, HDPE begins to neck at axial strains on the order of 10%. Within the neck, the axial strain henceforth varies with axial position on the specimen, and, with the displacement gradient no longer constant, the concept of a gage length becomes obsolete. Digital image correlation was thus used to measure directly the pointwise displacements and displacement gradients. Local axial, lateral and volumetric strains were calculated from the displacement gradients.

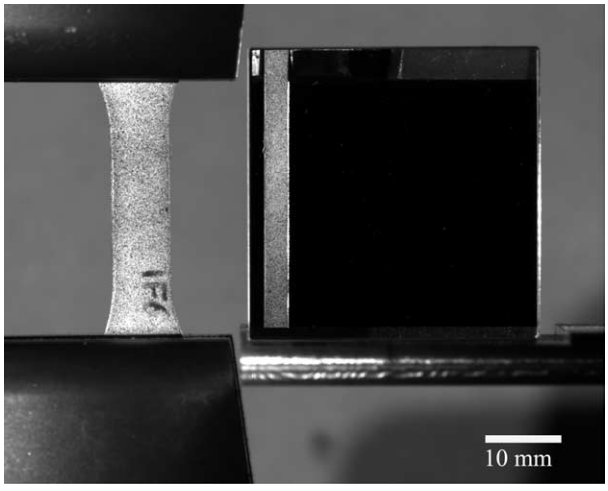


Fig. 3. Specimen held between tensile machine grips (left) and right-angle prism (right).

Full-field contours were constructed in a two-step process from the local displacements.

The images were analyzed with a DIC algorithm developed by Correlated Solutions Incorporated (CSI).[1] To correlate the reference image to the deformed images, the area of interest in the reference image is divided into small square subsets. The discrete matrix of the pixel gray level values in each subset forms a unique pattern within the image. As detailed in Parsons et al. [1], Schreier et al. [13], and Schreier and Sutton [14], second-order, two-dimensional shape functions, $u(x,y)$ and $v(x,y)$, from the front view, and $v(y,z)$ and $w(y,z)$, from the side view, map the positions within the reference subset to positions within each deformed image. The displacements and displacement gradients at the subset center are calculated by evaluating the shape functions and their partial derivatives at the subset center. This algorithm was used to determine the local displacements and strains at individual points on the specimen. Image resolution was 37.5 pixels/mm, and the subsets measured 51 pixels×51 pixels.

#### 2.3.1. Local strain calculation

Local lateral, axial and volumetric strains were calculated directly from the derivatives of the second-order mapping functions described above. Formally, the derivatives define the two-dimensional displacement gradients from the front and side views, respectively,

$$[\mathbf{H}_\mathrm{F}] = \begin{pmatrix} \frac{\partial u}{\partial x} & \frac{\partial u}{\partial y} \\ \frac{\partial v}{\partial x} & \frac{\partial v}{\partial y} \end{pmatrix} \text{and } [\mathbf{H}_\mathrm{S}] = \begin{pmatrix} \frac{\partial v}{\partial y} & \frac{\partial v}{\partial z} \\ \frac{\partial w}{\partial y} & \frac{\partial w}{\partial z} \end{pmatrix}. \quad (1)$$

The two-dimensional deformation gradients from the front and side views, respectively,

$$\mathbf{F}_\mathrm{F} = \mathbf{H}_\mathrm{F} + \mathbf{I} \text{ and } \mathbf{F}_\mathrm{S} = \mathbf{H}_\mathrm{S} + \mathbf{I}, \quad (2)$$

where $\mathbf{I}$ is the identity matrix, are thus known. (In general, $\mathbf{F}$ is defined as $\mathbf{I}+\mathrm{Grad}\,\mathbf{u}(\mathbf{x})$, where $\mathbf{x}$ is the position vector of a point in the reference configuration, and $\mathbf{u}(\mathbf{x})$ is the displacement of that point.) From the polar decomposition, $\mathbf{F}=\mathbf{VR}$, where $\mathbf{V}$ is the left stretch tensor and $\mathbf{R}$ is the rotation tensor, the true strain in the spatial configuration, or Hencky strain, is calculated for each view as

$$\mathbf{E} = \ln \mathbf{V}. \quad (3)$$

The volumetric strain $E_{kk}$ is defined as

$$E_{kk} = \ln\left(\frac{V}{V_0}\right) = \ln(\det \mathbf{F}_\mathrm{FS}), \quad (4)$$

where $V$ is the current volume, $V_0$ is the original volume, and $\mathbf{F}_\mathrm{FS}$, constructed from $\mathbf{H}_\mathrm{F}$ and $\mathbf{H}_\mathrm{S}$, is an approximation

[1] West Columbia, SC, 29169, USA. Tel.: +1 803 926 7272; url: www.correlatedsolutions.com.

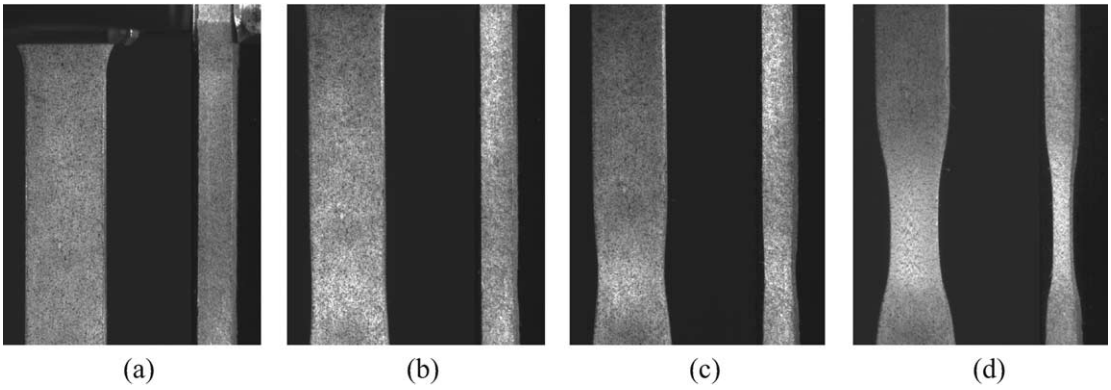


Fig. 4. Images of a 10%-filled HDPE tensile bar under uniaxial tension at increasing crosshead displacement, $U$: (a) reference (undeformed) image, (b) $U=6.3$ mm, (c) $U=10.1$ mm, (d) $U=20.0$ mm. Within each image, the front view is on the left, and the (inverted) side view is on the right.

of the three-dimensional deformation gradient at the specimen's edge.

Parsons et al. [1] showed previously that the local volumetric strain is most accurately calculated by approximating the pointwise deformation gradient from a cubic volume element at the edge of the specimen. Therefore, as shown in Fig. 5, the components of $\mathbf{F}_{FS}$ are taken partially from a front-view subset and partially from a side-view subset. The two subsets are at identical $y$-coordinates and have a common edge. $\partial v/\partial y$ is taken from the front view, and $\partial u/\partial z$ and $\partial w/\partial x$ are assumed to be zero, giving

$$[\mathbf{F}_{FS}] = \begin{pmatrix} \frac{\partial u}{\partial x}+1 & \frac{\partial u}{\partial y} & 0 \\ \frac{\partial v}{\partial x} & \frac{\partial v}{\partial y}+1 & \frac{\partial v}{\partial z} \\ 0 & \frac{\partial w}{\partial y} & \frac{\partial w}{\partial z}+1 \end{pmatrix}. \tag{5}$$

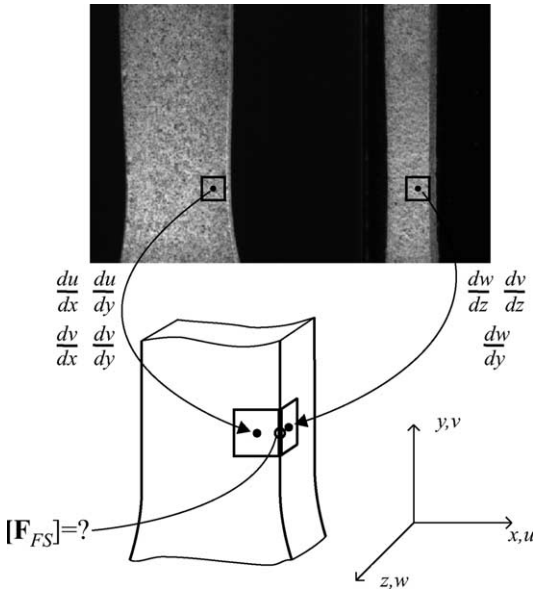


Fig. 5. Data from adjacent subsets on the front and side of the specimen is combined to form $\mathbf{F}_{FS}$ in order to calculate the volumetric strain.

*2.3.2. Full-field strain calculation*

With displacement and strain data available everywhere on the two visible sides of the specimen, strain can be studied simultaneously as a function of both position and time. Plotting contours of strain over the course of a tensile test illustrates clearly the localization process and allows ready comparison between different materials.

Contours of true axial strain were constructed from the displacement fields. Within the areas of interest, correlations were performed on pixel subsets of size $35\times35$ at a horizontal and vertical step size of two. The displacement of the center point of each subset was calculated and stored. The displacement of every second pixel in the area of interest was thus known. Subsets of the displacement field of size 11 points $\times$ 11 points were then taken at a horizontal and vertical step size of three. A temporary $(\tilde{x},\tilde{y})$ (front view) or $(\tilde{y},\tilde{z})$ (side view) coordinate system was translated to the center of each displacement field subset. Second-order polynomial expressions for $u(\tilde{x},\tilde{y})$ and $v(\tilde{x},\tilde{y})$, or $v(\tilde{y},\tilde{z})$ and $w(\tilde{y},\tilde{z})$, were fit by least-squares approximation to each displacement field subset. Similarly to the procedure described in Section 2.3.1, the displacement gradient, $\mathbf{H}_F$ or $\mathbf{H}_S$, was constructed from the partial derivatives evaluated at each subset center. The logarithmic strain, $\mathbf{E}=\ln\mathbf{V}$, was then calculated and plotted to form the full-field contours.

*2.4. True stress calculation*

True stress–true strain behavior is one of the most fundamental properties of a structural material. As discussed in the introduction, localization and dilatation complicate significantly its measurement in polymers under uniaxial tension. It is true that, if the volumetric strain is minimal, true stress–true strain can be accurately measured in compression with traditional methods. With the specimen cross-sectional area increasing with axial strain, compressive deformation is inherently stable and does not localize. Many polymers, however, behave differently in tension than in compression. Even neat, incompressible

polymers show a pressure dependence of yield, and those that craze or fragment will do so more readily under tension. Furthermore, particles in filled polymers are more likely to cavitate or debond during tensile deformation. Finally, even the most ductile polymers eventually fail, and the stress and strain at fracture can only be measured in tension. Thus, for most polymers, measuring the true stress–true strain behavior in tension is essential for complete understanding of the material's properties.

At any cross-section, the stress and strain vary across the width and thickness of the specimen. While the local lateral strains can be measured, there is no way to determine the local stresses. An average (or 'macroscopic') true stress for the whole specimen is, therefore, calculated from the total load and the current cross-sectional area of the specimen. (All macroscopic quantities are indicated by a variable with an overbar.) The macroscopic true stress, $\bar{T}_{yy}$, was calculated as

$$\bar{T}_{yy} \equiv \frac{P}{A} = \frac{P}{A_0 \bar{\lambda}_{xx} \bar{\lambda}_{zz}}, \tag{6}$$

where $P$ is the load cell measurement, $A$ is the current cross-sectional area of the specimen at the axial location where the neck forms, $A_0$ is the initial cross-sectional area of the specimen, and $\bar{\lambda}_{xx}$ and $\bar{\lambda}_{zz}$ are the macroscopic lateral stretches. $\bar{\lambda}_{xx}$ and $\bar{\lambda}_{zz}$ were calculated, respectively, from the specimen's overall width in the $x$-direction, $W$, and the specimen's overall thickness in the $z$-direction, $T$. From the front view, as shown in Fig. 6,

$$\bar{\lambda}_{xx} = \frac{W}{W_0} = \frac{X_L - X_R}{x_L - x_R}, \tag{7}$$

where, since DIC can only provide information at the center of a pixel subset,

$$X_L \approx x_L + u(x_c, y_c)_L + \frac{\partial u}{\partial x}\Big|_{(x_c,y_c)_L}(x_L - x_{cL}) \tag{8}$$

and

$$X_R \approx x_R + u(x_c, y_c)_R + \frac{\partial u}{\partial x}\Big|_{(x_c,y_c)_R}(x_R - x_{cR}). \tag{9}$$

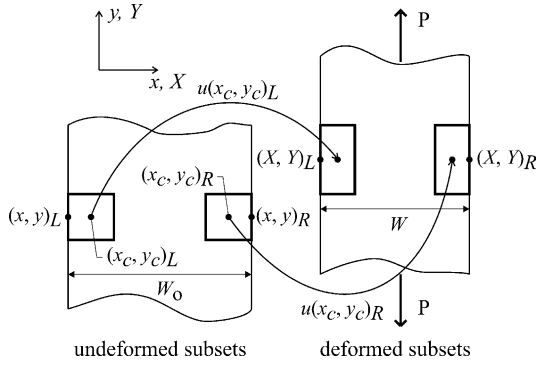


Fig. 6. Definition of variables used in the true stress calculation. Reference coordinates are denoted by $(x, y)$ and deformed coordinates are denoted by $(X, Y)$.

Here, we project the positions of the edges of the specimen from the positions of the centers of the left-most and right-most pixel subsets and the displacement gradients at those same locations. Analogously, from the side view,

$$\bar{\lambda}_{zz} = \frac{T}{T_0} = \frac{Z_L - Z_R}{z_l - z_r}, \tag{10}$$

and so forth.

## 3. Results

### 3.1. Full-field strain contours

Fig. 7 shows contours of true axial strain, $E_{yy}$, for a 10%-filled HDPE tensile bar at increasing crosshead displacements, $U$. The plots depict an isometric view of an initially 12.7 mm long section of the gage length. The corresponding load versus crosshead displacement data is shown in Fig. 8. The results clearly illustrate the three-dimensional necking phenomenon.

The plots of axial strain in Fig. 7 show that the specimen at first deforms uniformly. At $U=3.1$ mm (a), corresponding to the peak of the load–displacement curve, the axial strain is approximately constant at $E_{yy}=0.08$, indicating that the deformation is still predominantly homogeneous. At $U=6.3$ mm (b), the load is decreasing as localization occurs, and the strain field becomes non-uniform. The specimen narrows in the $x$ and $z$ directions, forming the neck. The site of neck initiation is the axial cross-section where, due to some geometric or morphological feature of the specimen, localization occurs first. Localization continues in the neck because the decrease in load carried at this section reduces the load on the rest of the specimen. Apparent in Fig. 7(b)–(d) are the gradients in strain which complicate the measurement of tensile true stress–true strain. In Fig. 7(d), the strain ranges from $E_{yy}=0.2$ to 0.6 over an axial distance on the order of the specimen width. The deformation remains concentrated in this region until the material strain hardens sufficiently for the neck to stabilize. The yield strength of the material, increasing with

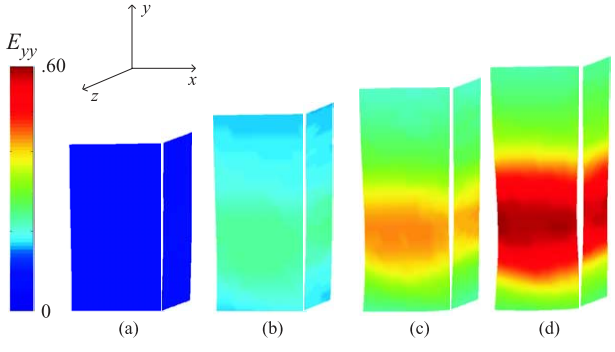


Fig. 7. Uniaxial tension of 10%-filled HDPE. Contours of true axial strain, $E_{yy}$, for increasing crosshead displacement, $U$: (a) $U=3.1$ mm, (b) $U=6.3$ mm, (c) $U=8.7$ mm, (d) $U=10.1$ mm.

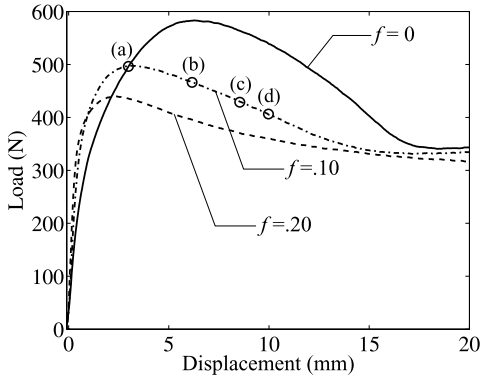


Fig. 8. Uniaxial tension of neat and calcium carbonate-filled HDPE. Load, $P$, versus crosshead displacement, $U$. ○ Denotes a displacement at which a contour is plotted in Fig. 7.

strain, must catch up with the counteracting effect of the decreasing cross-sectional area of the specimen. Only then is the deformation able to spread to an adjacent section.

A relevant observation is that localization occurs in this particular material by an essentially symmetric narrowing of the specimen. In some polymers, such as the neat polycarbonate studied by Parsons et al. [1], an approximately 45° shear band develops during neck formation.

### 3.2. Lateral versus axial strain

Fig. 9 shows the macroscopic true lateral strain versus true axial strain relationship for 10%-filled HDPE from both the front and side views. The macroscopic true lateral strains are calculated from the specimen's dimensions as $\bar{E}_{xx} = \ln \bar{\lambda}_{xx}$ and $\bar{E}_{zz} = \ln \bar{\lambda}_{zz}$, with $\bar{\lambda}_{xx}$ and $\bar{\lambda}_{zz}$ defined by Eqs. (7) and (10), respectively. For $\bar{E}_{xx}$, the true axial strain, $E_{yy}$, is taken at the lateral center of the specimen from the front view, while, for $\bar{E}_{zz}$, $E_{yy}$ is taken at the lateral center of the specimen from the side view. All strains are measured at the axial location where necking initiates. Readily apparent from a plot of axial strain versus time, the axial strain measures from each view are identical at any given instant. Up to an axial strain of approximately 0.4, the lateral versus axial strain is nearly the same in both specimen dimensions.

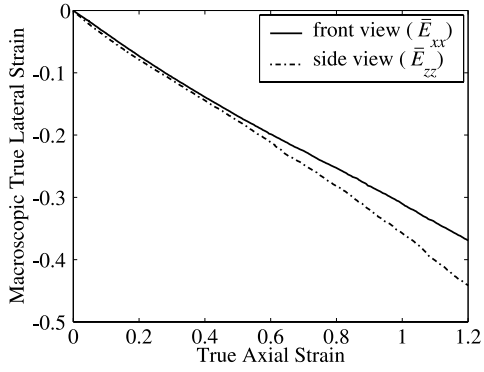


Fig. 9. Uniaxial tension of 10%-filled HDPE. Macroscopic true lateral strains, $\bar{E}_{xx}$ and $\bar{E}_{zz}$, versus true axial strain, $E_{yy}$.

The specimen shrinks in the lateral directions as it elongates in the axial direction, exhibiting an elastic Poisson's ratio of approximately 0.35. Beyond $E_{yy} = 0.4$, $\bar{E}_{zz}$ becomes larger in magnitude than $\bar{E}_{xx}$ as the specimen contracts more in the thinner $z$-direction than it does in the wider $x$-direction. The difference between $\bar{E}_{xx}$ and $\bar{E}_{zz}$ increases with increasing axial strain. At large axial strains, it is thus necessary to measure the strains in all three dimensions to calculate accurately the true stress and volumetric strain. The assumption of transversely isotropic deformations does not hold past axial strains of approximately 0.4. As an illustration of the magnitude of error which can be introduced if strains are measured in only two dimensions, Fig. 10 shows the volumetric strain for 10%-filled HDPE calculated in three different ways:

(1) using front-view data only and assuming transverse isotropy,
(2) using side-view data only and assuming transverse isotropy,
(3) using both front-view and side-view data to construct $\mathbf{F}_{FS}$ in Eq. (4).

It is apparent that using data from just one view can result in errors in inferred volumetric strain of up to 30%.

### 3.3. True axial stress–strain

Fig. 11 displays the macroscopic true stress–true strain results for neat HDPE and HDPE with 10% and 20% filler particles. All three materials are very ductile and draw to large strains. The macroscopic true stress is calculated from Eq. (6), and the true axial strain is taken from the front-view lateral center of the specimen. All strains are calculated at the axial location on the specimen where necking initiates. Taking first the result for $f = 0$, we see an initial linear region followed by a roll-over as yield occurs and then a slowly increasing strain hardening slope. It is apparent (and tabulated in Table 1) that the modulus increases with

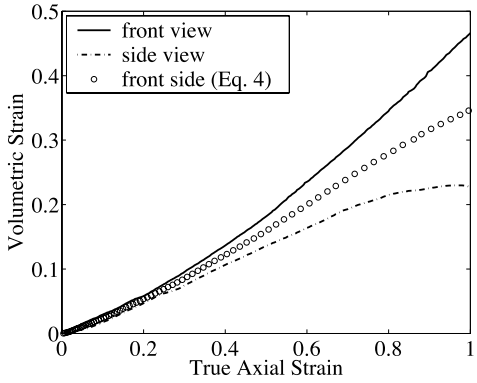


Fig. 10. Uniaxial tension of 10%-filled HDPE. Volumetric strain, $E_{kk}$, calculated with and without the assumption of transversely isotropic deformations, versus true axial strain, $E_{yy}$.

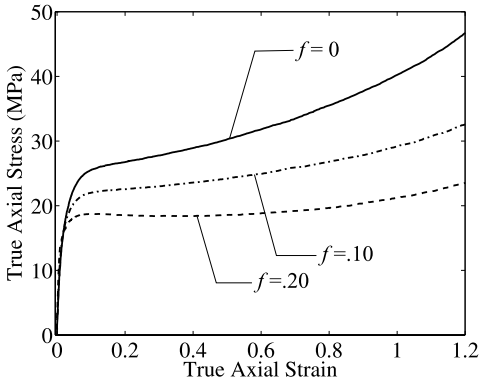


Fig. 11. Uniaxial tension of neat and calcium carbonate-filled HDPE. Macroscopic true axial stress, $\bar{T}_{yy}$,, versus true axial strain, $E_{yy}$.

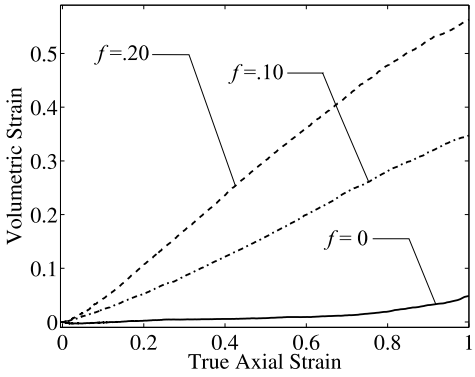


Fig. 12. Uniaxial tension of neat and calcium carbonate-filled HDPE. Volumetric strain, $E_{kk}$, versus true axial strain, $E_{yy}$.

increasing $f$, but the yield stress (taken at the axial strain where the peak load occurs) decreases with increasing $f$.

From the true stress–true strain data, a clear picture of the particles' effects emerges. Initially, the particles are well-bonded and act to reinforce the matrix, resulting in composites stiffer than neat HDPE. Soon, however, before yield in the interparticle volumes of matrix material (or matrix 'ligaments'), the local stresses at the matrix–particle interfaces exceed the adhesive strength of the interface, and the particles debond. The debonded particles essentially act as holes in the matrix, reducing the effective (load-bearing) cross-sectional area of the specimen. The stress in the matrix ligaments thus increases, the matrix yields, and the stress–strain curve rolls over. With lower flow stresses than the homopolymer, the composites' stress–strain behavior resembles that of a porous or compliant-particle modified material. As $f$ increases, debonding occurs at a lower macroscopic stress. The matrix ligaments are more highly stressed with increasing $f$, and yield occurs at a decreasing macroscopic stress as well.

After yield is where the advantages of the current technique truly become apparent. In sharp contrast to load-extension data where neither the true stress nor the true strain can be found, we are able, without assumption or approximation, to measure the true stress during plastic flow to tensile true strains exceeding 1.0 (an axial stretch of 2.7). Both the flow stress and the strain hardening slope decrease with increasing filler volume fraction. The neat polymer begins to strain harden immediately after yield, and the strain hardening slope gradually increases with increasing axial strain. The blend with $f=0.10$ behaves similarly but exhibits less strain hardening than the homopolymer. At $f=0.20$, however, there is a slight amount of strain softening before strain hardening begins. The trend in the results agrees with the experiments of Parsons et al. [1] and the micro-mechanical models of Socrate and Boyce [15] and Danielsson et al. [16] on neat and rubber-filled polycarbonate.

Table 1
Elastic modulus and yield stress of neat and calcium carbonate-filled HDPE

| F | Young's modulus (MPa) | Yield stress (MPa) |
|---|---|---|
| 0 | 1160 | 25.6 |
| 0.10 | 1660 | 21.9 |
| 0.20 | 2052 | 18.6 |

### 3.4. Volumetric strain

The volumetric strain results reinforce the conclusions drawn from the true stress–true strain data. There is overwhelming evidence of particle debonding and void growth. The volumetric strain, calculated from Eq. (4), in neat HDPE and the two blends is displayed in Fig. 12. Neat HDPE exhibits very little volume change, even in the elastic regime, with increasing axial strain. We conclude that crystal fragmentation does not occur at these strain levels, indicating that any volumetric strain in the filled materials must be due solely to particle debonding. Dilatation increases with increasing $f$. Exceedingly large volumetric strains are achieved when the particles debond and, as shown in the SEM micrograph[2] in Fig. 13, elongated cavities form around the particles. The enormity of the measured volumetric strains is attributed to the particles preventing inter-particle ligaments from 'pinching in'. Multi-particle micro-mechanical modeling has shown this effect to be exacerbated by particle clustering [17]. We note that similar trends in volumetric strain were reported by Lazzeri et al. [18] for calcium carbonate-filled polypropylene (which deformed in a homogeneous manner and thus lent itself to traditional extensometry methods).

### 3.5. Strain rate effects

Fig. 14 shows how the local true axial strain rate, $\dot{E}_{yy}$, at the axial location where necking begins, varies over the course of each test. ($\dot{E}_{yy}$ was simply taken as the slope of the

[2] Reprinted from Polymer, vol. 40, Bartczak Z, Argon AS, Cohen RE, Weinberg M, 'Toughness mechanism in semi-crystalline polymer blends: II. High-density polyethylene toughened with calcium carbonate filler particles', p. 2347–2365, 1999, with permission from Elsevier.


Fig. 13. SEM micrograph taken in the necked region of a calcium carbonate-filled HDPE ($f$=.25) tensile specimen from Bartczak et al. [11].

front-view $E_{yy}$ versus time curve.) The initial local strain rate is slightly less than predicted due to the effects of system compliance. The machine crosshead velocity is constant, but, as the deformation localizes, the strain rate in the neck increases. The displacement of the crosshead is accommodated almost entirely by a small section of the specimen gage section. Eventually, the strain rate peaks and begins to decrease as the deformation gradually spreads to regions adjacent to the neck. The maximum strain rate decreases with increasing $f$, indicating that the particles reduce the severity of material localization. This effect can also be seen in the load versus displacement plots of Fig. 8, where the load drop decreases with increasing $f$. A similar phenomenon was observed in rubber-filled polycarbonate by Parsons et al. [1]

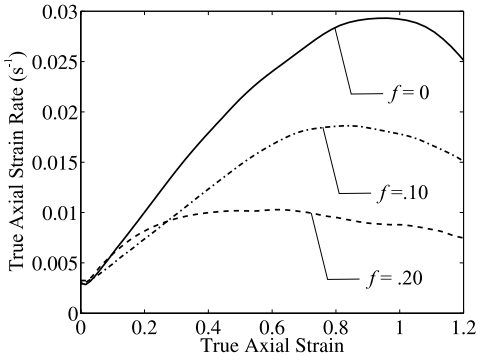


Fig. 14. Uniaxial tension of neat and calcium carbonate-filled HDPE. True axial strain rate, $\dot{E}_{yy}$, versus true axial strain, $E_{yy}$ at the axial location where necking begins.

The stress–strain and volumetric strain data presented in the previous two sections only approximates the constant strain rate behavior of the materials. Parsons et al. presented a data reduction strategy that minimizes the change in strain rate during a test by acquiring data at axial locations where the strain rate is closest to a chosen target strain rate. Up to the strains measured in this study, however, the variation in strain rate in neat HDPE and the blends is gradual and was found not to affect the results significantly. Therefore, in this study, all data was acquired at the axial location where necking began.

## 4. Discussion

A new method for simultaneously measuring strains in all three dimensions during a uniaxial tension test was introduced. Used in conjunction with digital image correlation, the technique was shown to measure successfully full-field strains, true stress–true strain, and volumetric strain in neat and rigid-filled polymers.

Experimental full-field strain contours provide valuable information about deformation mechanisms. As illustrated in Section 3.1, they quantify not only the degree of localization but also the modes of deformation–axial stretching versus shear banding in this case. In the previous study, Parsons et al. [1] showed, using full-field contours of axial strain, that the addition of rubber particles dramatically reduces localization in polycarbonate and shifts the mode of deformation from shear banding to pure axial stretching. The ability to measure full-field strains has great potential for assessing the toughness of polymers. The primary way to toughen polymers is to increase the volume of material involved in the plastic deformation process prior to fracture. Full-field strain contours of notched tension or notched bend tests would provide a quantitative measure of the extent of deformation in the vicinity of the notches before fracture.

True stress–true strain measurement is the most useful way to characterize the mechanical performance of a ductile polymer. True stress–true strain data is necessary for material selection, material tailoring and design, fitting constitutive models, and the development of new constitutive models. Measuring the response in tension is particularly important because micromechanisms such as crazing, crystal fragmentation, and particle debonding activate differently in tension than in compression. The triumvirate of localization, dilatation and anisotropic transverse deformations make measuring true stress–true strain in tension an arduous task, however. The technique used in this study was able to overcome these difficulties and obtain excellent data to large axial strains. The results show that particle debonding occurred at relatively low stress levels, causing

the blends to yield at a stress lower than that of the neat polymer. What was more interesting and unique to this study were the results after yield. A clear trend of decreased rate of strain hardening with increasing $f$ was apparent. In fact, at $f=0.20$, strain softening actually occurred.

Volumetric strain is a quantity critical for the complete understanding of polymer behavior. In glassy polymers, it is an indicator of crazing and, in semi-crystalline homopolymers, it is a sign of crystal fragmentation. In filled polymers, volumetric strain is also a symptom of particle debonding or particle cavitation. In this study, the immense volume change exhibited by the calcium carbonate-filled materials is proof that particle debonding and void growth are underlying physical processes contributing to the true stress–true strain results.

By capturing the deformation on adjacent sides of the specimen simultaneously, the current technique removes all uncertainty from the analysis. Contours of strain can be studied in three dimensions, and the assumptions of transverse isotropy and/or constant volume are not necessary. A potential source of significant error has thus been eliminated. Furthermore, by requiring but a single camera, the technique requires only slightly more equipment and labor than the largely two-dimensional technique introduced in the previous communication.

## Acknowledgements

This research was supported by the US Army through the Institute for Soldier Nanotechnologies, under Contract DAAD-19-02-D-0002 with the US Army Research Office. The content does not necessarily reflect the position of the Government, and no official endorsement should be inferred. We would like to thank Correlated Solutions (West Columbia, SC) for providing software specific to our needs and a pre-release version of their commercial product, 'Vic-2D.' Product details and contact information can be found at the CSI website, www.correlatedsolutions.com.

## References

[1] Parsons E, Boyce MC, Parks DM. Polymer 2004;45:2665–84.
[2] Thio YS, Argon AS, Cohen RE. Polymer 2004;45:3139–47.
[3] Buisson G, Ravi-Chandar K. Polymer 1989;31:2071–6.
[4] G'Sell C, Hiver JM, Dahoun A, Souahi A. J Mater Sci 1992;27:5031–9.
[5] Nazarenko S, Bensason S, Hiltner A, Baer E. Polymer 1994;35:3883–91.
[6] Haynes AR, Coates PD. J Mater Sci 1996;31:1843–55.
[7] Gloaguen JM, Lefebvre JM. Polymer 2001;42:5841–7.
[8] G'Sell C, Hiver JM, Dahoun A. Int J Sol Struct 2002;39:3857–72.
[9] Laraba-Abbes F, Ienny P, Piques R. Polymer 2003;35:3883–91.
[10] Bartczak Z, Argon AS, Cohen RE, Weinberg M. Polymer 1999;40:2331–46.
[11] Bartczak Z, Argon AS, Cohen RE, Weinberg M. Polymer 1999;40:2347–65.
[12] Roux, DC, Cooper-White, JJ, McKinley, GH, Tirtaatmadja, V. Phys Fluids 2003;15(9):S12.
[13] Schreier HW, Braasch JR, Sutton MA. Opt Eng 2000;39:2915–21.
[14] Schreier HW, Sutton MA. Exp Mech 2002;42:303–10.
[15] Socrate S, Boyce MC. J Mech Phys Solids 2000;48:233–73.
[16] Danielsson M, Parks DM, Boyce MC. J Mech Phys Solids 2002;50:351–79.
[17] Parsons E, Boyce MC, Parks DM (in preparation).
[18] Lazzeri A, Thio YS, Cohen RE. J Appl Polym Sci 2004;91:925–35.